Chapter 2: Chemical-Scale Studies on the Role of a Conserved Aspartate in Preorganizing the Agonist Binding Site of the Nicotinic Acetylcholine Receptor*

2.1 Introduction

2.1.1 The Nicotinic Acetylcholine Receptor

Neuroreceptors are central players in synaptic transmission, receiving and interpreting chemical signals between neurons in the nervous system. Neuroreceptors of the ligand-gated ion channel (LGIC) family directly convert incoming chemical signals into electrical output. In the LGIC gating process, neurotransmitters are recognized by ligand-binding domains, and binding triggers conformational changes within the structure to form an ion-conducting pore.

The nicotinic acetylcholine receptor (nAChR) has served as a prototype for understanding the structure and function of the Cys-loop family of LGICs (also known as pentameric LGICs). In this superfamily of receptors, which also includes γ-aminobutyric acid, glycine, and serotonin receptors, the five subunits are symmetrically or pseudosymmetrically arranged around a central ion-conducting pore. Each subunit contains a four-helix transmembrane domain that contains the ion channel gate and an extracellular ligand-binding domain. Members of the nAChR family are expressed at the neuromuscular junction and in the electric organ of eels and rays (muscle-type receptors), as well as in the central nervous system (neuronal receptors). The muscle-type receptor

is the best characterized, and the form studied here is the embryonic muscle nAChR, with a subunit stoichiometry of two α1 subunits and one each of the β1, γ, and δ subunits[1]. The nAChR has two agonist binding sites located at the α/γ and α/δ subunit interfaces[2–4]. The α subunits contribute the primary binding site components, termed loops A, B, and C, while the γ and δ subunits contribute the complementary components, primarily loop D (with possible contributions from loops E and F). The focus of this chapter is on loops A and B of the α subunit.

Work over the past several years on acetylcholine binding protein (AChBP) orthologs from mollusks has led to important new insights into the structures of Cys-loop receptor ligand-binding domains[5–8]. AChBP is a soluble, homopentameric protein produced in glial cells that is homologous to the nAChR ligand-binding domain. Crystal structures of AChBP with various agonists bound have established that the nAChR binding site is comprised of a box of conserved aromatic residues. One of these conserved aromatic residues is a tryptophan on loop B, W149 (Figures 2.1 and 2.2). Previous studies by this lab established that this tryptophan makes a strong cation-π interaction with ACh in the muscle-type receptor [9], and its role as a component of the AChBP "aromatic box" confirmed those findings. Subsequent work showed that the potent nicotinic agonist epibatidine also makes a cation-π interaction with W149 [9,10]. Nicotine is a quite weak agonist at the muscle-type receptor and does not form a cation-π interaction; its actions at the neuronal receptors are more substantial.

2.1.2 Previous Studies of D89/Loop B Interactions

The AChBP crystal structures suggest other important ligand-binding domain interactions that require verification through experiment. One structurally interesting interaction involves a conserved aspartate on loop A, D89[6]. This residue is part of a highly conserved WxPD motif exhibited across the entire Cys-loop superfamily (Figure 2.1). In the crystal structures of AChBP, D89 is positioned to interact with loop B through any of a number of hydrogen bonds between the aspartate carboxylate side chain and loop B residues T148, W149, and T150 (Figure 2.2). For the purposes of discussion, a schematic of the putative hydrogen bonding network, with potential hydrogen bonds labeled, is shown in Figure 2.3a. The high degree of conservation of the WxPD motif and the clear interaction of D89 with a known component of the agonist binding site (loop B/W149) have generated considerable interest in D89. Note that loop A also contains a canonical contributor to the aromatic box, Y93.

	loop A	loop B
AChBP	SL**W**V**PD**LAAYN	IG**SWT**H
mmα1	KI**W**R**PD**VVLYN	LG**TWT**Y
hα7	QI**W**K**PD**ILLYN	FG**SWS**Y
hGly- α1	SI**W**K**PD**MFFVH	IE**SY**AY
h5-HT_3A	SI**W**V**PD**ILINE	FE**SYS**H

Figure 2.1. Alignment of loops A and B for several Cys-loop receptors. The WxPD motif of loop A and the region around W149 of loop B are highlighted in red and blue, respectively. AChBP: ACh binding protein from *Limnaea stagnalis*; mmα1: nAChR α 1 subunit of mouse muscle (studied here); hα7: human nAChR α7 subunit; hGly- α1: human glycine receptor α1 subunit; h5-HT_3A: human 5-HT_3 A subunit. Y93 shown in green in the mmα1 sequence.

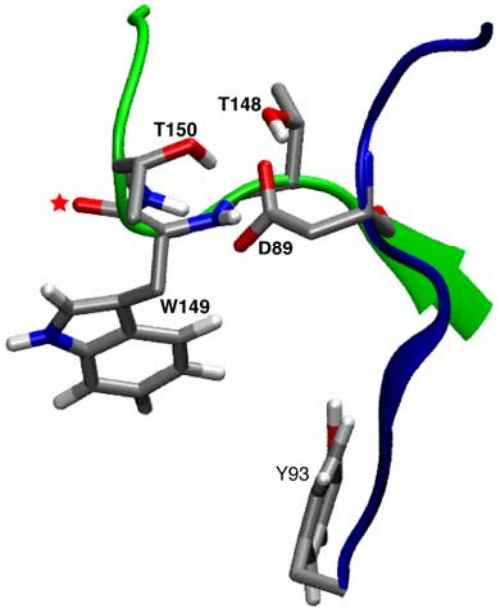

Figure 2.2. Region investigated in the Chapter 2 study. Loop A is shown in blue; loop B in green. Highlighted are the side chains of D89, T148, and T150, which together can form a network of hydrogen bonds. Also shown are contributors to the agonist binding site: Y93 from loop A; W149 side chain and W149 backbone carbonyl (red star) from loop B. This carbonyl and the side chain of Trp 149 point directly at the agonist, which in this view lies "behind" loop B. This image results from MD simulations, as discussed in text.

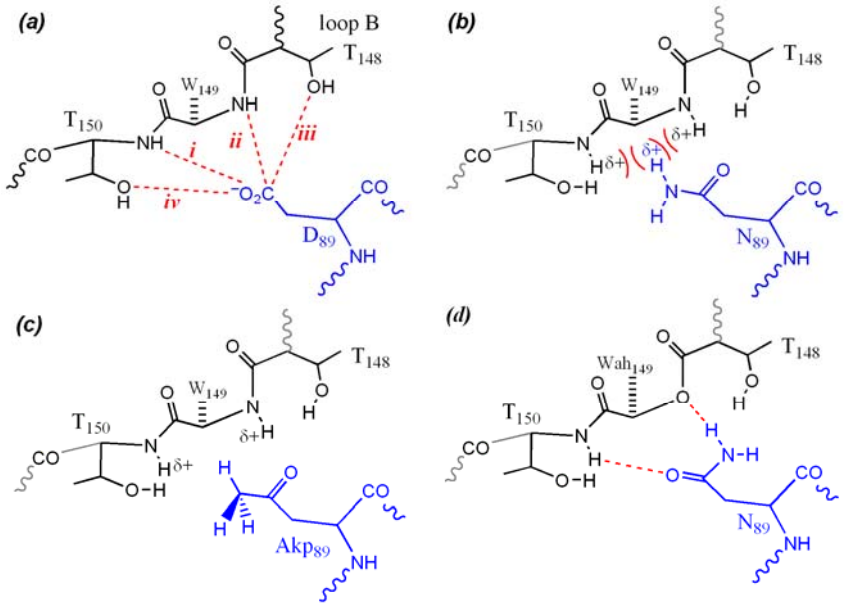

Figure 2.3. Schematics of potential hydrogen bonding interactions between loops A (blue) and B (black). ***(a)*** The wild type receptor. ***(b)*** D89N, highlighting the potential electrostatic clash. ***(c)*** D89Akp; note the lack of an electrostatic clash. ***(d)*** The double mutant D89N/W149Wah; note how hydrogen bond *ii* could, in principle, be restored.

Recently, Lee and Sine[11] have investigated D89 and its role in agonist binding by combining site-directed mutagenesis with single-channel kinetic analyses. Neutralization of the negative charge at position 89 through a mutation to asparagine or threonine, (D89N and D89T, respectively) substantially compromised receptor function, producing significant decreases in the bimolecular forward rate constant for agonist-receptor binding. In contrast, mutating residues T148 and T150, singly and in combination, did not seriously impact function. From these results, Lee and Sine concluded that D89 plays a structural role in stabilizing loop B, in particular W149, for agonist association. They concluded that essential structural features of the D89/loop B network were the negative charge of D89 and hydrogen bonds between the aspartate carboxylate and the amide backbones of T150 and T149 (hydrogen bonds *i* and *ii* in Figure 2.3a). They also proposed that a possible polarization of the backbone carbonyl of W149 contributes to ACh binding[6].

2.1.3 Project Goals

In the present study, we sought to further probe the role of the conserved D89 in the nAChR ligand-binding domain. Through the incorporation of unnatural amino acids using two different suppression methodologies[12–15], we introduced more subtle modifications to the side chain of D89, allowing what we have termed "chemical-scale" studies of such complex receptors. By chemical scale we mean, in effect, the distance scale to which chemists are accustomed: the functional group, the specific bond rotation or local conformational change, or the precise noncovalent interaction. We have also

incorporated amide-to-ester backbone mutations into loop B to probe proposed hydrogen bonds to this region. We conclude that the significantly disruptive D89N mutation affects receptor function in several ways: a distortion of the hydrogen bonding network, the introduction of an electrostatic clash between the asparagine amide side chain and the backbone amides of loop B, and, to a lesser extent, a neutralization of charge. We also find that, of the network of hydrogen bonds implied by the AChBP structure (Figure 2.3a), no one hydrogen bond is singularly important. Rather, maintaining the overall network of hydrogen bonds and avoiding electrostatic and/or steric clashes are essential for proper function. To support our unnatural amino acid mutagenesis studies, we conducted molecular dynamics simulations of the wild-type and D89N mutant ligand-binding domains in an effort to evaluate the hydrogen bonding network.

2.2 Results

2.2.1 Conventional Mutants, D89N and D89E

In this project, we evaluated receptors using the macroscopic parameter EC_{50}, the effective concentration of agonist necessary to achieve half-maximal response, rather than the more information rich, but more time consuming, single-channel analyses of Lee and Sine[11]. We made this choice both to examine a large number of mutants and to avoid the additional challenges of performing single-channel studies at the low expression levels often associated with unnatural amino acid mutagenesis. Of course, EC_{50} is a composite value that could be influenced by changes in agonist affinity or in gating. Since the mutations we are evaluating are proximal to the agonist binding site and are

quite remote from the gate of the channel, we interpret changes in EC_{50} as affecting binding more than gating. Consistent with this view, single-channel analyses of several D89 mutants reveal much more substantial changes in binding parameters than in gating parameters[11].

For comparison, we first studied two conventional mutants, D89N and D89E, that were also studied by Lee and Sine. The D89E mutant produced a modest 4-fold increase in EC_{50} for both ACh and epibatidine. However, the D89N mutant produced substantial 23- and 28-fold increases in EC_{50} for ACh and epibatidine, respectively (Table 2.1). Our results parallel the single-channel work, in which D89N produced a significant decrease in rate constants for ACh association while D89E resulted in a modest decrease in association rates and barely any change in the overall agonist binding equilibria.

2.2.2 Unnatural Mutants, D89Nha and D89Akp

Unnatural amino acids were incorporated at D89 through frame-shift suppression, instead of nonsense suppression. We used the frame-shift methodology because of the high level of misacylated THG73 incorporation at this position. Currents with an average magnitude of 0.29 ± 0.03 μA (Figure 2.4a) were observed when we performed the misacylation control experiment (injection of 74 nt THG73 tRNA). The dose-response relationship for this misacylation current (EC_{50} = 1.2 ± 0.1 μM; Figure 2.4b) suggested that Asp or Glu may have been the amino acid on the misacylated tRNA. When we performed a similar control experiment with the frame-shift suppressor tRNA, YFaFS, we observed negligible misacylation currents (0.05 ± 0.01 μA; Figure 2.4a).

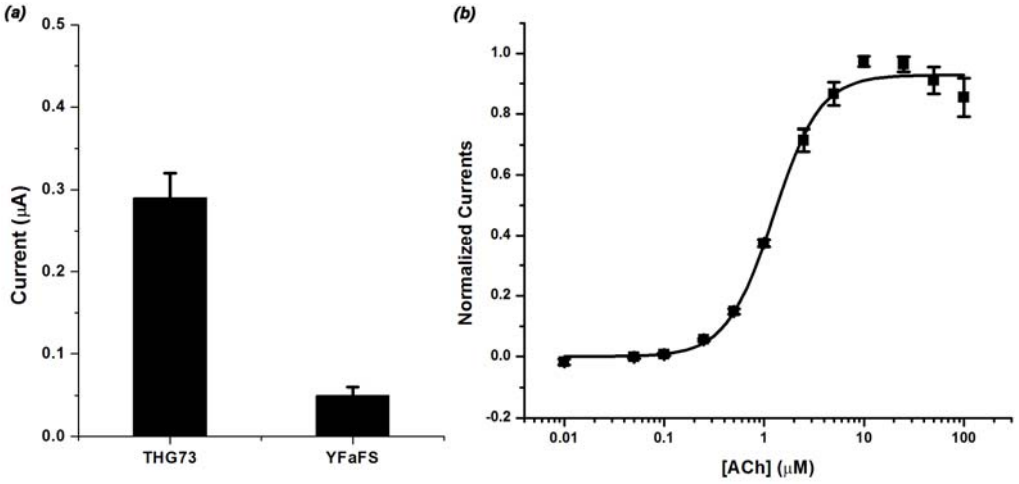

Figure 2.4. D89 misacylation data. ***(a)*** Comparison of currents from the misacylation control experiment for nonsense suppression (injection of 74 nt THG73 tRNA) and frame-shift suppression (injection of 74 nt YFaFS tRNA). Currents were 0.29 ± 0.03 μA for THG73 (N = 13) and 0.05 ± 0.01 μA for YFaFS (N = 5). ***(b)*** Dose-response relationship for misacylated THG73 currents. Hill equation parameters: EC_{50} = 1.2 ± 0.1 μM, n_H = 1.9 ± 0.2, N = 6 cells

The essential role of D89 is confirmed by the large perturbation of the D89N mutant. While generally considered a subtle change, an Asp-to-Asn mutation does more than simply neutralize charge. It also replaces a hydrogen-bond-accepting O atom with a hydrogen-bond-donating NH_2 group, and in the context of this system, this change introduces a possible electrostatic clash between position 89 and loop B (Figure 2.3b). The amide side chain of asparagine places an $N^{\delta-}$–$H^{\delta+}$ bond dipole proximal to the $N^{\delta-}$–$H^{\delta+}$ bond dipoles of the loop B amide backbone at T150 and W149. This possible repulsive interaction between the $N^{\delta-}$–$H^{\delta+}$ dipoles could contribute to the deleterious effects of the D89N mutant.

In an attempt to dissect these two features of the D89N mutant, we incorporated two unnatural amino acids that neutralize the negative charge of Asp without introducing an electrostatic clash. A nitro group (NO_2) is isoelectronic and isosteric to a carboxylate, but it has no negative charge (Figure 2.5). Also, a nitro group is a substantially weaker

hydrogen bond acceptor than carboxylate[16]; the measured difference in energetics of carboxylate and nitro hydrogen bonding is 1.5–2.0 kcal/mol[17], corresponding to a factor of 10–20 in an equilibrium constant. The ideal residue would be nitroalanine (Noa), the nitro analog of Asp, but it is not chemically compatible with the nonsense suppression methodology (see Appendix A for details). Therefore, we studied nitrohomoalanine (Nha), the nitro analog of Glu (Figure 2.6). Since the D89E mutant produces only a modest change in receptor function, comparing the Nha mutant to the Glu mutant was deemed meaningful.

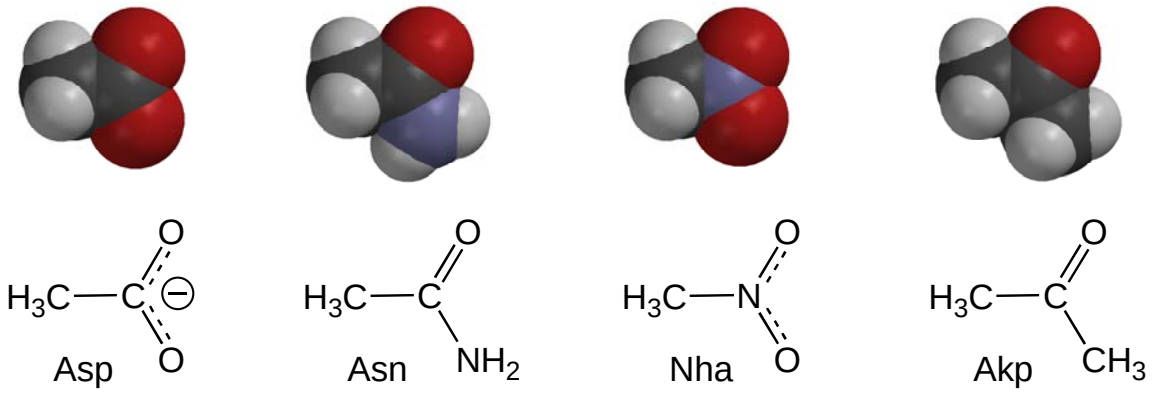

Figure 2.5. Functionalities of side chains used in Chapter 2. Space-filling models shown. Note the greater steric similarity between Asp and Nha and between Asn and Akp.

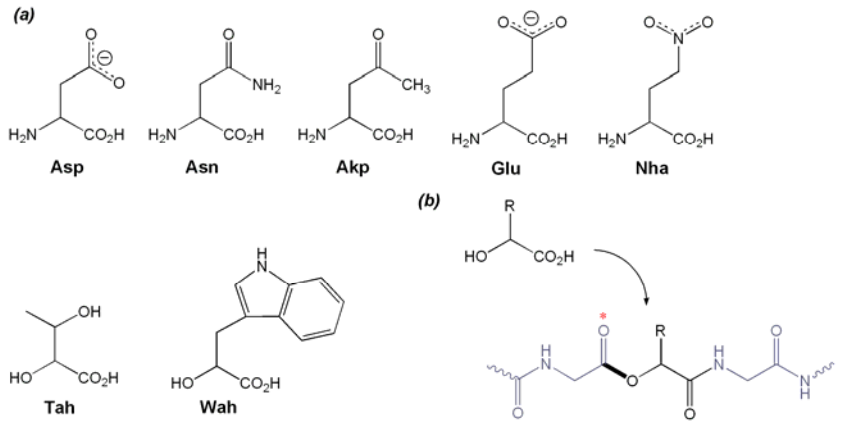

Figure 2.6. Structures of hydroxyl acids, natural, and unnatural amino acids used in Chapter 2. ***(a)*** Natural and unnatural amino (and hydroxy) acids structures. ***(b)*** Consequences of incorporating an α-hydoxy acid into a protein. The critical ester linkage is highlighted in bold; the carbonyl that is modulated is noted with a star.

Table 2.1. D89 Mutants[a]

		Wild Type[b]	D89N[b]	D89E[b]	D89Nha	D89Akp
ACh	EC_{50}	0.83 ± 0.04	19 ± 1	3.4 ± 0.3	14 ± 1	8.0 ± 0.7
	n_H	1.8 ± 0.1	1.6 ± 0.1	1.6 ± 0.1	1.3 ± 0.1	1.7 ± 0.2
	N	22	8	9	8	5
Epi	EC_{50}	0.60 ± 0.04	13 ± 1	2.4 ± 0.1	11 ± 1	5.0 ± 0.5
	n_H	1.6 ± 0.1	2.0 ± 0.2	1.7 ± 0.2	1.7 ± 0.3	1.5 ± 0.2
	N	22	5	3	8	5

[a]EC_{50} (μM) and Hill coefficient ± standard error of the mean. The receptor has a Leu9'Ser mutation in M2 of the β subunit. [b]Data reported previously[10,18]

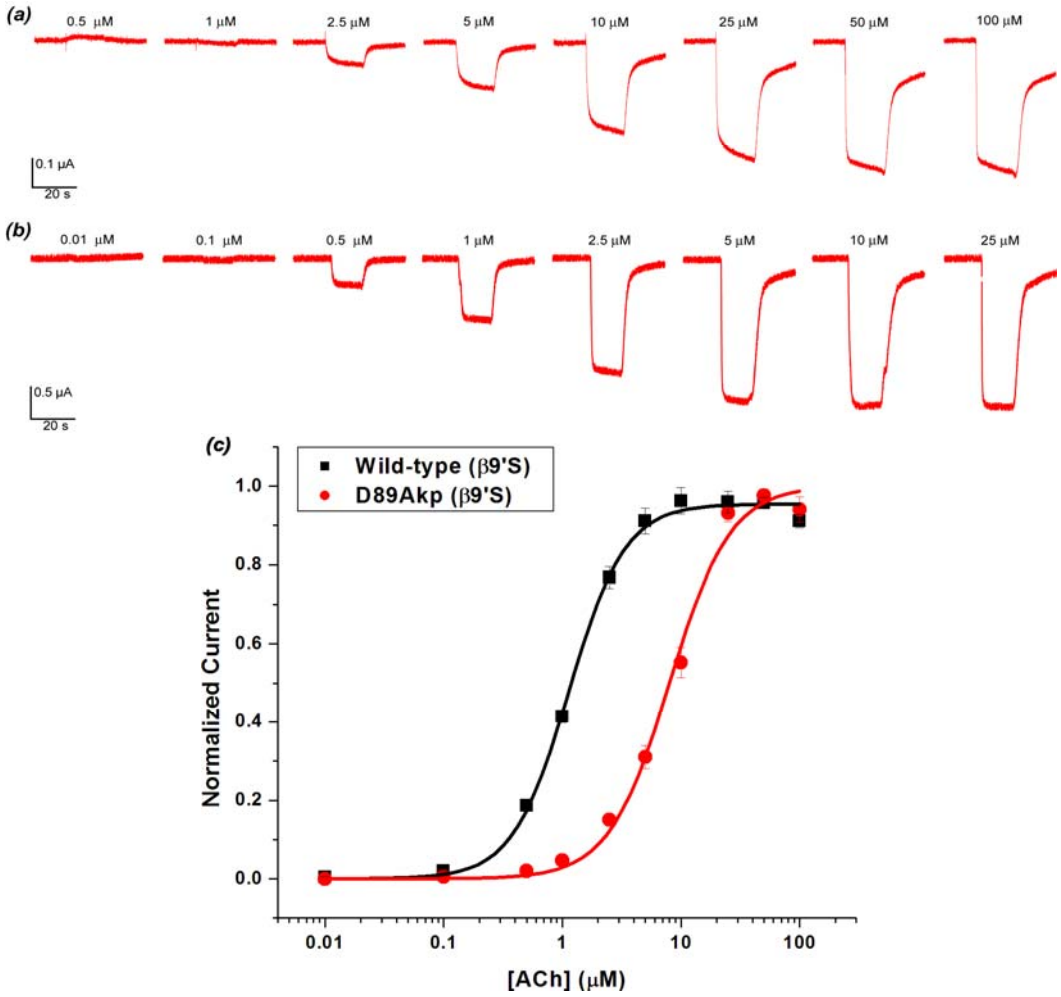

Figure 2.7. Representative dose-response relationships for D89Akp ***(a)*** and D89 wild-type recovery ***(b)***. ***(c)*** Data from same conditions as ***(a)*** and ***(b)*** fit to the Hill equation

Incorporation of Nha at position 89, D89Nha, resulted in a modest 4-fold increase in EC_{50} when compared to that of the isosteric D89E receptor for both ACh and

epibatidine (Table 2.1). This change is comparable to that of the original D89E mutation. The D89Nha mutant behavior suggests that charge neutralization is no more deleterious than an increase in side chain length at position 89.

The second neutral unnatural amino acid we incorporated was 2-amino-4-ketopentanoic acid (Akp; Figure 2.6), producing D89Akp. Akp is a direct analog of Asp, and the ketone side chain of Akp is sterically similar to the Asp and especially the Asn side chains (Figure 2.5 and 2.6). However, Akp lacks the $N^{\delta-}$–$H^{\delta+}$ bond dipole (Figure 2.3c), and so does not contribute an electrostatic clash. When Akp was incorporated at position 89, 8- and 10-fold increases in EC_{50} were observed for ACh and epibatidine, respectively, relative to that of wild type (Table 2.1 and Figure 2.7). The ~ 2.5-fold difference in EC_{50} between the D89Akp and D89N receptors can be attributed to the electrostatic clash produced by the Asn $N^{\delta-}$–$H^{\delta+}$ dipole.

Table 2.2. Nicotine Data[a]

	Wild Type[b]	**D89E**[b]	**D89N**[b]	**D89Nha**	**D89Akp**
EC_{50}	57 ± 2	59 ± 6	1600	270 ± 60	110 ± 10
n_H				1.9 ± 0.5	2.7 ± 0.6
N				9	5

[a]EC_{50} (μM) and Hill coefficient ± standard error of the mean. The receptor has a Leu9'Ser mutation in M2 of the β subunit. [b]Data reported previously[18]

These two unnatural amino acid mutations were also studied with nicotine as the agonist. While nicotine is a full agonist at neuronal receptors, it is a weak partial agonist at the muscle type of nAChR. Incorporation of Nha produced a 4.5-fold shift in nicotine EC_{50} relative to that of the D89E mutant, and the incorporation of Akp produced an almost 2-fold shift relative to that of wild-type (Table 2.2). (Unlike ACh and epibatidine, the D89E mutation did not shift the nicotine EC_{50}; the wild-type nicotine EC_{50} was 57 ± 2

μM and the the D89E mutant EC_{50} was 59 ± 6 μM[18].) The negative charge of Asp appears to be of equal importance to nicotine as it is with ACh and epibatidine. But, when compared to the D89N mutation (EC_{50} = ~ 1600 μM[18]), the slight shift in EC_{50} caused by the D89Akp mutation suggests that the electrostatic clash of Asn affects nicotine binding more than ACh and epibatidine.

2.2.3 Loop B Backbone Mutations

Of the four possible hydrogen bonds in the D89/loop B network, two involve side-chain–to–side-chain interactions, and two involve hydrogen bonds with the loop B amide backbone (Figure 2.3a). The side chain interactions (*iii* and *iv*) have been probed by conventional mutagenesis[11]. T148L, T150A, and T148L/T150A mutants were not substantially disruptive, suggesting hydrogen bonds *iii* and *iv* are not crucial. By inference, backbone hydrogen bonds *i* and *ii* have been proposed to be especially critical to receptor function[11].

Table 2.3. Loop B and Double Mutants[a]

		Wild Type	**T150Tah**	**W149Wah**	**D89N**	**D89N / T150Tah**	**D89N / W149Wah**
ACh	EC_{50}	0.83 ± 0.04	0.25 ± 0.01	0.81 ± 0.03	19 ± 1	15 ± 1	2.2 ± 0.1
	n_H	1.8 ± 0.1	1.4 ± 0.04	1.6 ± 0.1	1.6 ± 0.1	1.4 ± 0.2	1.8 ± 0.1
	N	22	17	7	8	7	6
Epi	EC_{50}	0.60 ± 0.04	2.2 ± 0.2	1.6 ± 0.1	13 ± 1	2.9 ± 0.3	0.76 ± 0.05
	n_H	1.6 ± 0.1	1.3 ± 0.1	1.6 ± 0.1	2.0 ± 0.2	1.2 ± 0.1	1.7 ± 0.1
	N	22	16	5	5	6	6

[a] EC_{50} (μM) and Hill coefficient ± standard error of the mean. The receptor has a Leu9'Ser mutation in M2 of the β subunit. Data reported previously[10,18]

Probing backbone hydrogen bonds requires the power of unnatural amino acid mutagenesis. Appropriate amide-to-ester mutations remove the backbone NH group that

can contribute to the hydrogen bond (Figure 2.6b). In this system, the T150Tah mutation disrupts hydrogen bond *i*, and the W149Wah mutation disrupts hydrogen bond *ii*. The W149Wah mutation produced very modest effects (Table 2.3), suggesting that hydrogen bond *ii* is nonessential.

The T150Tah mutation has been studied previously[10]. It is unique among the mutations considered here in that the results for ACh and epibatidine are qualitatively different; the EC_{50} for ACh decreased ~ 3-fold, while that for epibatidine increased ~ 4-fold. Ester backbones not only eliminate a hydrogen bond donor in the backbone, but also weaken the corresponding (adjacent) carbonyl as a hydrogen bond acceptor. The carbonyl perturbed by the T150Tah mutation, the W149 backbone carbonyl (*star* in Figures 2.2 and 2.6b), points away from the region being probed here and directly into the agonist binding site. Epibatidine can make a hydrogen bond to this carbonyl, and the ester mutation weakens the hydrogen-bond-accepting ability of the carbonyl, accounting for the increase in EC_{50}. No such hydrogen bond is possible for ACh. As such, we consider ACh the better gauge of the importance of hydrogen bond *i*, and we ascribe a nonessential role for it.

2.2.4 D89N and Ester Double Mutants

Backbone ester mutations in loop B were also produced in an attempt to recover wild-type receptor function from the D89N mutant. If indeed a $N^{\delta-}$–$H^{\delta+}$•••$H^{\delta+}$–$N^{\delta-}$ dipole-dipole clash is introduced by the D89N mutation, an appropriate backbone ester would not only alleviate the clash, but would replace it with a potentially favorable

hydrogen bond (Figure 2.3d). Two double mutants were evaluated, D89N/T150Tah and D89N/W149Wah (Table 2.3). The D89N/T150Tah double mutant (attempting to rescue hydrogen bond *i*) did not fully recover wild-type receptor function: 18- and 5-fold increases in EC_{50} were observed for ACh and epibatidine, respectively. In contrast, the D89N/W149Wah double mutant (attempting to rescue hydrogen bond *ii*; Figure 2.3d) produced near wild-type activity, with EC_{50} increases of only 2.7- and 1.3-fold for ACh and epibatidine, respectively. These results suggest that there is an asymmetry in the D89/loop B network that allows the electrostatic clash of the Asn side chain to be relieved through an ester at position 149 but not at position 150. Note that the D89N/W149Wah mutant receptor is an example of a receptor that contains no negative charge in the vicinity of position 89, but retains nearly wild-type activity.

2.2.5 Molecular Dynamics Simulation of nAChR Ligand-binding Domain

We performed two simulations of the mouse muscle nAChR ligand-binding domain, one without and one with the agonist carbamylcholine (CCh) bound. Other simulations of AChBP and variants of the nAChR have appeared[19–24]. The agonist-free structure is based on Unwin's model of the receptor from *T. marmorata*, which is nearly identical in sequence to the mouse muscle receptor. CCh was then docked into this structure in a manner compatible with the crystal structure of AChBP that contains CCh in the agonist binding site[6]. We monitored hydrogen bonds *i* through *iv*, considering both oxygens of the D89 carboxylate (called OD1 and OD2; Figure 2.9), for a total of eight possible interactions. Along with the D89/loop B hydrogen bonds, we monitored two

"control" hydrogen bonds that are part of a well-defined α-helix in the ligand binding domain. The results summarized in Figure 2.8 and Table 2.4 are calculated from the final 500 ps of the 5 ns simulations.

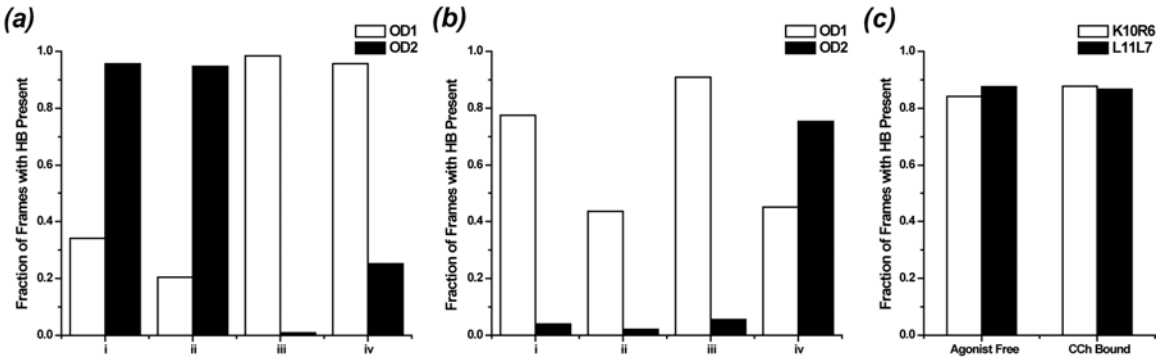

Figure 2.8. Analysis of hydrogen bonding in the molecular dynamics simulations of the nAChR ligand-binding domain without ***(a)*** and with ***(b)*** CCh bound. Hydrogen bonds were monitored between both D89 carboxylate oxygens (OD1, white bars, and OD2, black bars) and the four loop B hydrogen bond donors. ***(c)*** Control hydrogen bonds between the backbone amide of K10 and the backbone carbonyl of R6 (K10R6, white bar) and the backbone amide of L11 and the backbone carbonyl of L7 (L11L7, black bar) were also monitored in both structures. All observations were made during the last 500 ps of the 5 ns simulations. Data expressed as the fraction of the 1000 observed frames where a given hydrogen bond was present

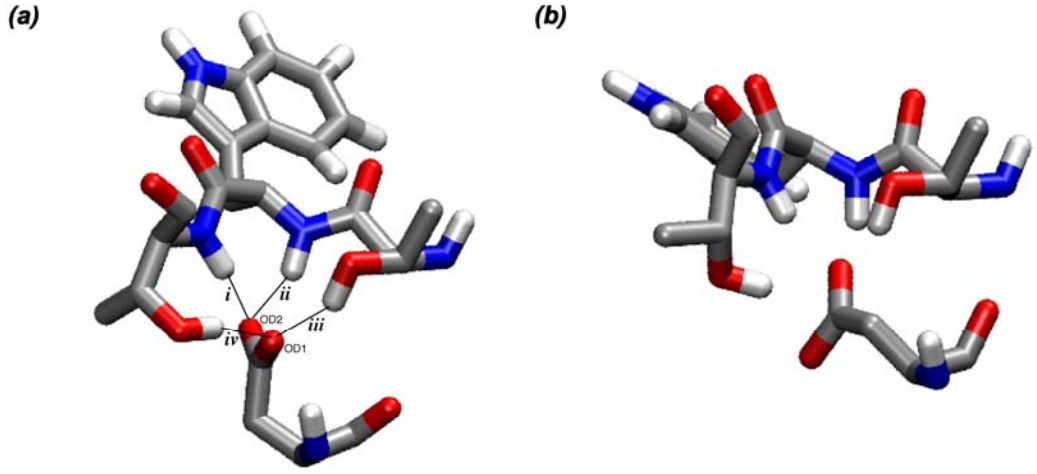

Figure 2.9. Two views of hydrogen bonding interactions for the receptor. Structure without ***(a)*** and with ***(b)*** CCh bound shown. Generated with the g_cluster program of the GROMACS suite from the final 500 ps of the 5 ns nAChR ligand-binding domain simulations

Table 2.4. Molecular Dynamics Simulations[a]

	D89-Loop B Distance (Å)[b]	Number of D89-LoopB Hydrogen Bonds[c]	rmsd[d]
WT Agonist Free	4.3 ± 0.2	4.7 ± 0.8	--
WT CCh Bound	5.2 ± 0.3	3.4 ± 0.8	1.5 ± 0.2
D89N1	5.3 ± 0.3	1.6 ± 0.6	2.5 ± 0.1
D89N2	8.1 ± 0.5	1.5 ± 0.9	3.8 ± 0.3

[a]All statistics averaged over the last 500 ps of the given simulation (1000 frames) and presented as mean ± standard deviation of the mean. [b]Distance measured from D89 or N89 γ carbon to the W149 α carbon. [c]All hydrogen bonds between position 89 and loop B residues, T148, W149, and T150. Includes both oxygens of D89 in wild-type simulations. [d]rmsd calculated in reference to the average structure from the last 500 ps of the agonist free wild-type simulation. Average structure from g_cluster program of GROMACS suite

The agonist-free structure shows a very well-defined hydrogen bonding network. In a representative structure (Figure 2.9a), one carboxylate oxygen (OD2) makes hydrogen bonds to the two backbone NH groups (*i* and *ii*), while the other carboxylate oxygen makes hydrogen bonds to the two side chain OH groups (*iii* and *iv*). These are strong hydrogen bonds, being present more frequently than the reference hydrogen bonds of the α helix. Occasionally, one carboxylate oxygen simultaneously makes three hydrogen bonds; on average, there are 4.7 hydrogen bonds between D89 and loop B. Note that the orientation of the carboxylate in this simulation (Figure 2.2 and 2.9a) differs from previous models, the side chain having rotated to enable formation of four hydrogen bonds.

Addition of the agonist CCh leads to a weakened interaction between D89 and loop B. In the agonist-free simulation, D89 interacts with all four loop B hydrogen bond donors in 94% of the frames, but that number drops to 34% of the frames in the CCh-bound simulation. Hydrogen bonds to the loop B backbone, interactions *i* and *ii*, are

present less frequently in the CCh-bound structure (decreases of 17% and 50%, respectively, in the number of frames with a hydrogen bond present), while the side chain interactions, hydrogen bonds *iii* and *iv*, remain. The average number of hydrogen bonds drops from 4.7 to 3.4 when agonist binds, and the distance between D89 and W149 increases from 4.3 Å to 5.1 Å (measured from the D89 γ carbon to the W149 α carbon; Table 2.4). We also observed a similar decrease in hydrogen bonding between D89 and loop B when analyzing the last 500 ps of an α7 simulation[25] (3.97 ± 0.05 compared to 3.73 ± 0.05 hydrogen bonds for the agonist-free and CCh-bound structures, respectively). In the CCh-bound structure, OD1 makes the majority of the interactions with loop B, while OD2 only interacts with the T150 hydroxyl side chain (Figure 2.9b). Structurally, the changes between empty and occupied agonist binding sites arise because the D89 side chain rotates to a less symmetrical arrangement that favors one carboxylate oxygen over the other in hydrogen bonding (Figure 2.9). Also, the T150 side chain reorients, but the OH group ends up in a similar location. In addition, as others have noted, the side chain of W149 reorients to make a cation-π interaction with the agonist.

Simulations of the D89N mutant were performed on the agonist-free structure only, because the Asn mutant mainly affected the kinetics of association of the agonist with the unbound nAChR[11]. Two simulations that differ in the initial orientation of the Asn side chain were considered. In the D89N1 simulation, the N89 amide nitrogen was placed in a position comparable to that of OD1 of the agonist-free wild type structure, while in D89N2, the nitrogen was placed in the OD2 position.

As summarized in Table 2.4, both simulations show that the D89N mutant substantially disrupts the interaction between position 89 and loop B. The average

distance between N89 and loop B (measured from the N89 γ carbon to the W149 α carbon) over the final 500 ps was larger for both D89N1 and D89N2 simulations (5.3 Å and 8.1 Å, respectively) than either wild-type simulation. Also, in the D89N mutant simulations the 4.7 hydrogen bonds seen in the agonist free wild-type simulation are reduced to ~ 1.5, and many of these hydrogen bonds do not correspond to hydrogen bonds *i*–*iv*, but are new hydrogen bonds involving the backbone of N89. The substantial disruption of the D89N mutant structures was also observed in the loop B region. A comparison between the final loop B structure of the agonist-free wild-type simulation and comparable structures from the D89N1 and D89N2 simulations yielded rmsds of 2.5 Å and 3.8 Å, respectively (Table 2.4).

2.3 Discussion

2.3.1 AChBP and the D89/Loop B Network

The study of the nAChR ligand-binding domain has been transformed by information gained from the AChBP crystal structures. Structural interactions found in the AChBP crystal structures have served as a starting point for new mutation studies in the nAChR and other Cys-loop family receptors[26,27]. However, since the AChBP is not an actual LGIC and is < 25% homologous to the closest nAChR relative, α7, experiments are necessary to test the relevance of interactions found in the crystal structures. The use of unnatural amino acids has allowed us to probe the relevance of these AChBP interactions at a chemical scale unavailable with conventional mutagenesis[10,12,13,28].

In this study, we have evaluated the structural role of the highly conserved residue, D89. According to the AChBP crystal structures, D89 provides the contact point between loop A, which contains D89 and agonist binding site residue Y93, and loop B, which contains the critical agonist binding site residue W149 (Figure 2.2). In the AChBP structures the D89 carboxylate forms hydrogen bonds with the backbone amides of loop B residues T150 and W149, while also interacting with the hydroxyl side chains of T148 and T150. This network is conserved among the primary ligand-binding subunits of the Cys-loop family of receptors (Figure 2.1). As noted before, D89 is part of a highly conserved WxPD motif found in essentially all known Cys-loop receptors. The residues aligning with T148 are conserved as hydroxyl side chains, serine, or threonine. W149 is part of the conserved aromatic box that comprises the agonist-binding site. In three different Cys-loop receptors—the nAChR considered here, the 5-HT_3 (serotonin) receptor, and the $GABA_C$ receptor—the aromatic residue that aligns with W149 makes direct contact with a bound agonist through a cation-π interaction [9,10–28,29].

2.3.2 D89/Loop B Unnatural Amino Acid Mutations

The essential role of D89 was established by the severe consequences of the relatively modest mutation D89N, an effect reported previously[11]. Such a mutation could disrupt any or all of the four potential hydrogen bonds suggested by the AChBP structures (Figure 2.3). Conventional mutagenesis previously showed that hydrogen bonds *iii* and *iv* could be removed without significant disruption of receptor function. Using unnatural amino acid mutagenesis, we have now ablated hydrogen bonds *i*

(T150Tah) and *ii* (W149Wah), and neither change is seriously disruptive. Clearly, no single hydrogen bond between loop B and loop A is critical to receptor function.

Beyond disruption of the D89 / loop B hydrogen bond network, the D89N mutation neutralizes the negative charge of the wild-type Asp. Others have concluded that binding of cationic agonists such as ACh requires a negative charge in the loop A/loop B interface region. However, more subtle charge-neutralization strategies, such as incorporation of Nha or Akp, do not reproduce the full D89N effect. This suggests that another factor is operative.

We propose that the D89N mutation also introduces a destabilizing $N^{\delta-}$–$H^{\delta+}$•••$H^{\delta+}$–$N^{\delta-}$ dipole-dipole clash between position 89 and loop B. The other charge-neutralizing mutations, D89Nha and D89Akp, do not experience such a clash and so are less disruptive. Also, the introduction into the D89N mutant receptor of a second, backbone mutation that removes one of the offending $N^{\delta-}$–$H^{\delta+}$ dipoles (D89N/W149Wah) restores near wild-type behavior. This double mutant has no negative charge at the loop A / loop B interface yet is near wild type in behavior.

Nicotine data for the D89 mutations diverges from that of ACh and epibatidine, which are quite similar to each other. While the D89E and D89Akp mutants produce modest shifts in the ACh and epibatidine EC_{50}s, nicotine potency is barely affected. In contrast, the wild type to D89N and D89E to D89Nha nicotine EC_{50} shifts are similar to those for ACh and epibatidine (Figure 2.10).

The most glaring difference in the nicotine data is found when comparing the D89N and D89Akp EC_{50} shifts for each agonist (Electrostatic Clash in Figure 2.10).

There is a 14.5-fold improvement in nicotine potency when the Asn amide NH_2 group is substituted with the CH_3 group of Akp; ACh and epibatidine only experience a ~ 2.5-fold improvement. Relieving the electrostatic clash between Asn and loop B returns nicotine potency almost to that of wild type. Because ACh and epibatidine EC_{50} values are still quite shifted, we concluded that the Akp mutation still disrupts the loop B structure possibly through general steric perturbations or destruction of the symmetry of the D89 / loop B interactions. Because nicotine only makes one contact with loop B, a hydrogen bond to the W149 carbonyl[10], the loop B binding requirements for nicotine are fewer than for the stronger agonists, ACh and epibatidine. These observations suggest that ACh and epibatidine are more sensitive to perturbations in loop B structure than nicotine.

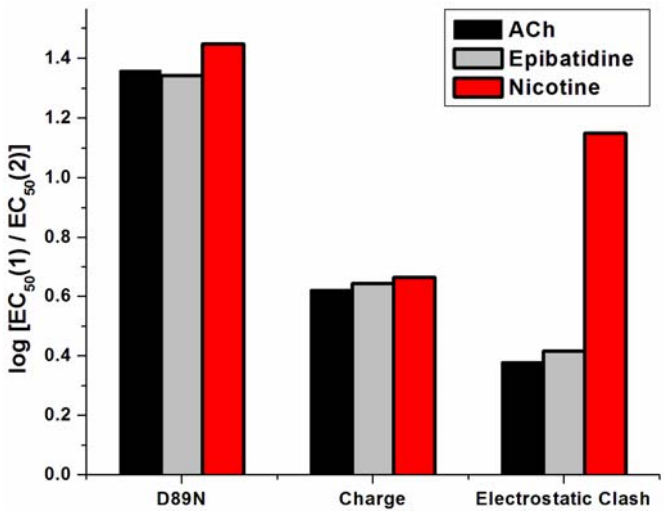

Figure 2.10. D89 unnatural mutation data compared between ACh, epibatidine, and nicotine. Three different EC_{50} comparisons are made for each agonist and plotted as the log of the ratio of the two EC_{50}s (log [EC_{50}(1) / EC_{50}(2)]). D89N: EC_{50}(1) is D89N and EC_{50}(2) is wild type; Charge: EC_{50}(1) is D89Nha and EC_{50}(2) is D89E; Electrostatic Clash: EC_{50}(1) is D89N and EC_{50}(2) is D89Akp.

2.3.3 D89N Mutation and Implications for the Role of D89 in Ligand Binding

Another proposed role for D89 is a polarization of the W149 carbonyl (*star* in Figure 2.2), which points into the agonist binding site and can directly contact agonists[6]. An amide carbonyl is highly polarized $C^{\delta+}=O^{\delta-}$, and the partial negative charge on oxygen could contribute to binding of cationic agonists. It has been proposed that the negative charge of D89 could enhance this polarization[6], although we are unaware of any precedent for this type of effect. Our results do not appear to support this suggestion. For the mutant T150Tah, the key carbonyl is much less polarized, as it is now an ester carbonyl rather than an amide carbonyl. However, this mutation decreases ACh EC_{50}, the opposite of expectations from the polarization suggestion.

The picture that emerges for the role of D89 is not simple. It seems certain that hydrogen bonding between the side chain of D89 and loop A is involved. However, no one interaction is singularly important. A subset of the full complement of interactions between D89 and loop B is required to stabilize the nAChR ligand-binding site.

Another possible indication of the disruptive nature of the D89N mutation can be found from a pair of Cys-loop receptors that are gated by serotonin. The 5-HT_3 receptor has a Trp that aligns with the nAChR Trp α149, and it makes a cation-π interaction with the agonist serotonin.[28] Interestingly, the MOD-1 receptor from *C. elegans* naturally contains the D89N modification, a rare exception to the highly conserved WxPD motif. Also, even though MOD-1 is highly homologous to the 5-HT_3 receptor, and binds the same neurotransmitter, the cation-π interaction in MOD-1 has moved away from the loop

B aromatic residue to a different residue in the aromatic box on loop C. [30] This could reflect the disruption of loop B caused by the D89N substitution in MOD-1.

Molecular dynamics simulations generally support the experimental data of others and ourselves. In our simulations, a sharp reduction in the level of hydrogen bonding in the position 89/loop B network suggests that the D89N mutation severely disrupts interactions between position 89 and loop B. In fact, in one of the D89N simulations, the Asn side chain ceases to interact at all with loop B. Both D89N mutant simulations produced loop B structures that differed from their wild type counterparts. From these observations we conclude that loop B adjusts in structure to accommodate the Asn.

From our molecular dynamics simulations of the mouse muscle nAChR ligand-binding domain, it appears that D89 interacts with loop B more in the agonist-free state than in the agonist-bound state. Relative to the agonist-free structure we find an average of approximately one fewer hydrogen bond between D89 and loop B; and D89 is almost 1 Å further from loop B in the CCh-bound structure. Because loop B itself does not relocate substantially on agonist binding (as revealed in the comparison of our agonist-free and CCh bound wild-type simulations), the role of D89 is to preorganize the empty agonist binding site into a conformation that favors binding, an effect that would enhance binding affinity[31]. Apparently, once the agonist is bound, the stabilization of loop B provided by D89 is no longer necessary, and the interaction between the two is weakened. This is consistent with an earlier conclusion that the D89N mutation affects agonist association but not subsequent steps in the channel activation mechanism[11].

In conclusion, chemical-scale studies of the D89/loop B network have further refined our understanding of this interesting and highly conserved structural feature. D89 and loop B form a redundant network of hydrogen bonding interactions, no one of which is essential. In addition, the charge on D89 is not essential for receptor function. The D89N mutation both disrupts the hydrogen bonding network and introduces a repulsive electrostatic interaction, significantly destabilizing the D89/loop B network. These results, along with molecular dynamics simulations and earlier single-channel studies[11], indicate that the role of the D89/loop B network is to preorganize the agonist binding site for ligand binding, with no significant contribution to the gating mechanism.

2.4 Materials and Methods

Unnatural Amino Acid Suppression

Synthetic amino acids and α-hydroxy acids were conjugated to the dinucleotide dCA and ligated to truncated 74 nt tRNA as previously described[32,33]. Aminoacyl tRNA was deprotected by photolysis immediately prior to co-injection with mRNA, as described previously[32,34]. Typically, 25 ng of tRNA was injected per oocyte along with mRNA in a total volume of 50 nL/cell. mRNA was prepared by *in vitro* runoff transcription using the Ambion (Austin, TX) T7 mMessage mMachine kit. The site of interest was mutated to the amber stop codon by standard means, verified by sequencing through both strands. Mouse muscle embryonic nAChR in the pAMV vector was used. A total of 4.0 ng of mRNA was injected in an α:β:γ:δ subunit ratio of 10:1:1:1. In all cases, a Leu-to-Ser mutation at a site 50 Å from the nAChR ligand-binding domain in the

M2 helix, known as 9', was used to lower EC_{50} values to a measurable range[10,28]. Previous work on this mutation has shown that a Leu9'Ser mutation in the β subunit lowers EC_{50} values 40-fold without changing trends in EC_{50} values[13,28]. In addition, the α subunits contain an HA epitope in the M3-M4 cytoplasmic loop for Western blot studies. Control experiments show that this epitope does not detectably alter EC_{50}. As a negative control for suppression, truncated 74 nt tRNA or truncated tRNA ligated to dCA was co-injected with mRNA in the same manner as fully charged tRNA. At the positions studied here, no current was ever observed from these negative controls. The positive control for suppression involved wild-type recovery by co-injection with 74 nt tRNA ligated to dCA-Thr or dCA-Trp. Frameshift suppression at αD89 was utilized as described by Rodriguez *et al*[35].

Electrophysiology

Stage V-VI oocytes of *Xenopus laevis* were employed. Oocyte recordings were made 24 to 48 h postinjection in two-electrode voltage clamp mode using the OpusXpress™ 6000A (Axon Instruments, Union City, CA). Oocytes were superfused with Ca^{2+}-free ND96 solution at flow rates of 1 mL/min before application, 4 mL/min during drug application, and 3 mL/min during wash. Holding potentials were -60 mV. Data were sampled at 125 Hz and filtered at 50 Hz. Drug applications were 15 s in duration. Acetylcholine chloride was purchased from Sigma/Aldrich/RBI. Epibatidine was purchased from Tocris as (±) epibatidine dihydrochloride. All drugs were prepared in sterile ddi water for dilution into calcium-free ND96. Dose-response data were

obtained for a minimum of 10 concentrations of agonists and for a minimum of three cells. Dose-response relations were fitted to the Hill equation to determine EC_{50} and Hill coefficient values.

Generation of Mouse Muscle nAChR Heteropentamer Computational Model

A model of the mouse muscle ligand-binding domain was created by first aligning the mouse muscle nAChR sequence with the sequence of the *Torpedo marmorata* acetylcholine receptor, the structure of which had been determined using electron microscopy by Unwin[36] and resolved to 4 Å resolution[37]. An alignment was generated using the T-Coffee website. A homology model was then built with this alignment using Prime[38], within the Schrödinger suite of programs. The individual chains of *Torpedo* structure 2BG9 were used as templates for each subunit type. Chain A of the Torpedo structure was used as a template for both α subunits of the mouse muscle nAChR. Each subunit was exported as a PDB file and aligned in Swiss PDB Viewer[39]. This structure was imported back to Prime where a side-chain prediction algorithm was used.

This heteropentamer was converted to GROMACS[40] format and inserted into a periodic box with 7 Å gaps between the protein and the box edge for molecular mechanics minimizations and simulations. SPC water molecules[40] were used to add explicit solvation to the model followed by the insertion of sodium and chloride ions to bring the molarity of the box to 150 mM. An excess of sodium ions was added to neutralize the charge of the protein.

Ligand Incorporation into Mouse Muscle nAChR Model

Using this heteropentamer, another structure was generated containing carbamoylcholine (CCh) in the ligand-binding pocket. CCh was inserted into the two binding pockets of the mouse muscle nAChR. This was performed by aligning the box residues of the mouse muscle model with the D binding site of the AChBP structure containing CCh (1UV6). Gromacs parameters for the ligand (CCh) were initially generated using ProDRG (http://davapc1.bioch.dundee.ac.uk/programs/prodrg/)[41]. The charges generated by ProDRG for CCh were modified due to a large positive charge that was inaccurately placed on the nitrogen atom of the ammonium. Instead, ChelpG charges from HF/6-31G** calculations were used with some attenuation of the partial charges between carbamoyl protons and oxygens to fit within GROMACS MD parameters.

Generation of the D89N Mutant Structures

D89N mutant structures were made from the homology model PDB file by mutating D89 of both α subunits to Asn using Swiss PDB. The two structures differed in their orientations of the NH_2 group of the side chain: D89N1 placed the NH_2 group in a position analogous to that of OD1 of D89 in the wild-type model, while D89N2 placed the NH2 group in a position analogous to that of OD2. The mutant models were then placed in a hexagonal periodic box and treated like the wild-type model.

Molecular Dynamics Simulations

All four nAChR structures (agonist free wild type, CCh bound wild type, D89N1, and D89N2) underwent one minimization step. Then, under the GROMACS force field, MD simulations were begun. The MD simulations started at 0 K and warmed to 310 K over the first 25 ps. The protein and drug (CCh bound structure) were highly restrained during this warmup, followed by 100 ps of slowly releasing the restraints. All simulations after this point continued unrestrained for 5000 ps (wild type-structures) or 7500 ps (D89N mutant structures). α7 model and molecular dynamics simulations were performed by E. James Petersson[25].

Analysis of Molecular Dynamics Simulations

All molecular dynamics trajectories were analyzed using the tools included in the GROMACS suite(*26*). All characterizations were performed on the last 500 ps of the simulations. Each trajectory file contained data for every 0.5 ps, yielding 1000 frames of analysis per simulation.

Distances and hydrogen bonds were analyzed using the g_dist and g_hbond programs, respectively. The default g_hond hydrogen bond structural cut-offs (a donor/acceptor distance of 3.5 Å and an acceptor-hydrogen-donor angle of 30°) were used when monitoring hydrogen bonds.

rmsd values for the CCh bound wild type, D89N1, and D89N2 simulations were calculated using the g_rms program. All comparisons were made with respect to the

average loop B structure of the last 500 ps of the agonist-free wild-type simulation obtained from g_cluster, using the gromos method and an rmsd cutoff of 0.14 Å. The α carbons of the two structures to be compared were aligned prior to the rmsd calculation. Figure 2.9 was produced from PDB files generated by g_cluster, using the conditions described above on the agonist free and CCh bound wild-type simulation trajectories.

Synthesis of Wah cyanomethyl ester and dCA-Wah

Syntheses for both molecules performed by Amanda L. Cashin[18].

Synthesis of t-Butyl 2-Diphenylmethyleneimino-4-nitro-butanoate, nitrohomoalanine, NVOC-nitrohomoalanine, NVOC-nitrohomoalanine cyanomethyl ester, and Nha-dCA

Described in Appendix A.

Synthesis of Akp-dCA

The synthesis of 2-amino-4-ketopentanoic acid and preparation of Akp-dCA were described previously[42].

2.5 References

(1) Miyazawa, A.; Fujiyoshi, Y.; Stowell, M.; Unwin, N. *Journal of Molecular Biology* **1999**, *288*, 765–786.

(2) Corringer, P.J.; Novere, N. L.; Changeux, J.-P. *Annual Review of Pharmacology and Toxicology* **2000**, *40*, 431–458.

(3) Grutter, T.; Changeux, J.P. *Trends in Biochemical Sciences* **2001**, *26*, 459–463.

(4) Karlin, A. *Nature Reviews Neuroscience* **2002**, *3*, 102–114.

(5) Brejc, K.; van Dijk, W. J.; Klaassen, R. V.; Schuurmans, M.; van der Oost, J.; Smit, A. B.; Sixma, T. K. *Nature* **2001**, *411*, 269–276.

(6) Celie, P. H. N.; van Rossum-Fikkert, S. E.; van Dijk, W. J.; Brejc, K.; Smit, A. B.; Sixma, T. K. *Neuron* **2004**, *41*, 907–914.

(7) Hansen, S. B., Sulzenbacher, G., Huxford, T., Marchot, P., Taylor, P., Bourne, Y. *EMBO Journal* **2005**, *24*, 3625–3646.

(8) Smit, A. B.; Syed, N. I.; Schaap, D.; van Minnen, J.; Klumperman, J.; Kits, K. S.; Lodder, H.; van der Schors, R. C.; van Elk, R.; Sorgedrager, B.; Brejc, K.; Sixma, T. K.; Geraerts, W. P. M. *Nature* **2001**, *411*, 261–268.

(9) Zhong, W.; Gallivan, J. P.; Zhang, Y.; Li, L.; Lester, H. A.; Dougherty, D. A. *PNAS* **1998**, *95*, 12088–12093.

(10) Cashin, A. L.; Petersson, E. J.; Lester, H. A.; Dougherty, D. A. *J. Am. Chem. Soc.* **2005**, *127*, 350–356.

(11) Lee, W. Y.; Sine, S. M. *J. Gen. Physiol.* **2004**, *124*, 555–567.

(12) Dougherty, D. A. *Current Opinion in Chemical Biology* **2000**, *4*, 645–652.

(13) Kearney, P. C.; Nowak, M. W.; Zhong, W.; Silverman, S. K.; Lester, H. A.; Dougherty, D. A. *Mol Pharmacol* **1996**, *50*, 1401–1412.

(14) Nowak, M. W.; Gallivan, J. P.; Silverman, S. K.; Labarca, C. G.; Dougherty, D. A.; Lester, H. A.; Conn, P. M. *Methods in Enzymology* **1998**, *293*, 504–529.

(15) Rodriguez, E. A.; Lester, H. A.; Dougherty, D. A. *Proc. Natl. Acad. Sci.* **2006**, *103*, 8650–8655.

(16) Kelly, T. R.; Kim, M.H. *Journal of the American Chemical Society* **1994**, *116*, 7072–7080.

(17) Thorson, J. S.; Chapman, E.; Schultz, P.G. *Journal of the American Chemical Society* **1995**, *117*, 9361–9362.

(18) Cashin, A. L. California Institute of Technology, 2006.

(19) Gao, F.; Bern, N.; Little, A.; Wang, H.L.; Hansen, S. B.; Talley, T. T.; Taylor, P.; Sine, S. M. *J. Biol. Chem.* **2003**, *278*, 23020–23026.

(20) Gao, F.; Bren, N.; Burghardt, T. P.; Hansen, S.; Henchman, R. H.; Taylor, P.; McCammon, J. A.; Sine, S. M. *J. Biol. Chem.* **2005**, *280*, 8443–8451.

(21) Henchman, R. H.; Wang, H.L.; Sine, S. M.; Taylor, P.; McCammon, J. A. *Biophys. J.* **2003**, *85*, 3007–3018.

(22) Henchman, R. H.; Wang, H.L.; Sine, S. M.; Taylor, P.; McCammon, J. A. *Biophys. J.* **2005**, *88*, 2564–2576.

(23) Le Novere, N.; Grutter, T.; Changeux, J.P. *PNAS* **2002**, *99*, 3210–3215.

(24) Schapira, M.; Abagyan, R.; Totrov, M. *BMC Structural Biology* **2002**, *2*, 1.

(25) Petersson, E. J. California Institute of Technology, 2005.

(26) Criado, M.; Mulet, J.; Bernal, J. A.; Gerber, S.; Sala, S.; Sala, F. *Mol Pharmacol* **2005**, *68*, 1669–1677.
(27) Mukhtasimova, N.; Free, C.; Sine, S. M. *J. Gen. Physiol.* **2005**, *126*, 23–39.
(28) Beene, D. L.; Brandt, G. S.; Zhong, W.; Zacharias, N. M.; Lester, H. A.; Dougherty, D. A. *Biochemistry* **2002**, *41*, 10262–10269.
(29) Lummis, S. C. R.; L. Beene, D.; Harrison, N. J.; Lester, H. A.; Dougherty, D. A. *Chemistry & Biology* **2005**, *12*, 993–997.
(30) Mu, T. W.; Lester, H. A.; Dougherty, D. A. *J. Am. Chem. Soc.* **2003**, *125*, 6850–6851.
(31) Cram, D. J. *Angewandte Chemie—International Edition in English* **1986**, *25*, 1039–1057.
(32) Nowak, M. W.; Gallivan, J. P.; Silverman, S. K.; Labarca, C. G.; Dougherty, D. A.; Lester, H. A. *Ion Channels, Pt B* **1998**, *293*, 504–529.
(33) England, P. M.; Lester, H. A.; Dougherty, D. A. *Tetrahedron Letters* **1999**, *40*, 6189–6192.
(34) Li, L. T.; Zhong, W. G.; Zacharias, N.; Gibbs, C.; Lester, H. A.; Dougherty, D. A. *Chemistry & Biology* **2001**, *8*, 47–58.
(35) Rodriguez, E. A.; Lester, H. A.; Dougherty, D. A. *PNAS* **2006**, *103*, 8650–8655.
(36) Miyazawa, A.; Fujiyoshi, Y.; Unwin, N. *Nature* **2003**, *423*, 949–55.
(37) Unwin, N. *J Mol Biol* **2005**, *346*, 967–89.
(38) Schrodinger, I. Portland, OR.
(39) Guex, N.; Peitsch, M. C. *Electrophoresis* **1997**, *18*, 2714–2723.
(40) van der Spoel, D., Lindahl, E., Hess, B., van Buuren, A.R., Apol, E., Meulenhoff, P. J., Tieleman, D.P., Sijbers, A.L.T.M., Feenstra, K.A., R., v.D., Berendsen, H.J.C. 2004.
(41) Schuettelkopf, A. W.; van Aalten, D.M.F. *Acta Crystal* **2004**, *D60*, 1355–1363.
(42) Mu, T. California Institute of Technology, 2006.